Terahertz photoconductivity and Photocarrier dynamics in few-layer hBN/WS_2 van der Waals heterostructure laminates

M. Bala Murali Krishna[1,3], Julien Madéo[1], Joel Pérez Urquizo[1], Xing Zhu[1], Soumya Vinod[2], Chandra Shekar Tiwary[2,4], Pulickel M. Ajayan[2], and Keshav M. Dani[1]

[1]Femtosecond Spectroscopy Unit, Okinawa Institute of Science and Technology Graduate University, 1919-1 Tancha, Onna-son, Kunigami, Okinawa 904-0495 Japan.

[2]Department of Materials Science and NanoEngineering, Rice University, Texas-77005, USA.

[3]School of Physical Sciences, Central University of Karnataka, Kadaganchi – 585367, India.

[4]Materials Science and Engineering, Indian Institute of Technology, Gandhinagar, Gujarat, India.

KEYWORDS: 2D materials, van der Waals heterostructures, Time resolved Terahertz spectroscopy, photoconductivity.

Abstract

Van der Waals (vdW) heterostructures is a rapidly emerging field that promises to produce on-demand properties for novel optoelectronic devices. Assembly of dissimilar two-dimensional atomic crystals in the vdW heterostructure enables unique features and properties which are fundamentally different from individual 2-dimensional (2D) crystals. Currently, most growth and fabrication methods prohibit large scale, micron-thick and robust heterostructures. An alternative approach is the one based on liquid phase exfoliation allowing the possibility of scalable thin films and composites. Such thin films have inherent and predicted advantages: they can display new behaviors due to their extremely high surface area and, as free-

standing laminates, can be manipulated with mixing of nanosheets and other materials for novel device attributes. We use the aforementioned route to prepare spray-coated and few microns thick WS_2 and hBN/WS_2 heterostructure laminates. A combination of photoluminescence and transmission electron microscope measurements show that, despite the disordered layer stacking inherent to the fabrication process, the laminates preserve the few layer optical response. In particular, the hBN/WS_2 heterostructure laminates exhibit a 3-layer average distribution. Using optical pump-terahertz probe (OPTP) measurement to access the photocarrier dynamics and photoconductivity, we study and compare the photocarrier dynamics and photoconductivity of pure WS_2 and hBN/WS_2 samples. The hBN/WS_2 samples show an unusual response different from what has been previously reported for pure transition metal dichalcogenides. After photoexcitation, instead of a monotonic decay as in pure WS_2, an initial fast decay is followed by a rise of the negative differential terahertz (THz) transmission dominating the dynamics for the following 50 ps. By analyzing the time resolved THz complex photoconductivity, we attribute this effect to the presence of free carriers as well as dipoles at the hBN/WS_2 interfaces. As previously reported in hBN/Graphene heterostructures, interfacial dipoles can form along with free carriers at the instant of photoexcitation. Whereas free carriers cause a decrease in the transient THz transmission due to Coulomb screening, dipoles can provide an increase in the pump-induced change in transmission. In terms of complex photoconductivity, free carriers have both real and imaginary components while dipoles probed off-resonance provide almost a purely imaginary response. Our results provide a deeper understanding of the photoconductive response of large van der Waals heterostructure laminates fabricated by liquid phase exfoliation, and will enable their use in future optoelectronic applications.

Introduction

The realization of van der Waals (vdW) heterostructures [1] has stimulated vigorous research efforts for their use in advanced electronic and optoelectronic devices. The diversity of the two-dimensional materials gives us a unique playground to design hybrid structures by combining dissimilar two-dimensional (2D) layers. The interlayer coupling between the different 2D layered materials in vdW heterostructures plays a

vital role in controlling their electronic and optical behaviors. Interesting questions arise as to how and what new features can emerge in heterostructures that differs from those of individual layers. Recent works have shown formation of charge transfer states and type II band alignment [2–10], in which photoexcited electrons and holes are confined to different layers of vdW heterostructures owing to strong interlayer interactions. A recent report [2] provides evidence of very rapid charge transfer (<50 fs) between interlayers using ultrafast pump-probe spectroscopy. These separated charge species in different layers have shown promising properties such as micron-scale drift-diffusion and long lasting valley population and polarization [11]. These kinds of artificial heterostructures have led to exciting progress in fundamental science [12–14] as well as bandgap-engineered devices for efficient LEDs and photodetectors [15,16]. The interlayer interactions in the 2D vdW heterostructures can also be engineered by intercalation of dielectric barrier layers in 2D semiconductors [17,18]. vdW heterostructures comprising intercalated dielectric layers or substrates show the emergence of an interfacial potential difference [17–21] and is essentially interpreted as a 2D dipole – an atomically thin parallel plate capacitor with vdW gap and built-in potential. The development of interfacial potential difference is due to the charge rearrangement led by the work function mismatch and Pauli exchange repulsion [19]. From this intercalation of dielectric layers in-between semiconducting or conducting 2D layers emerges novel properties due to modification of the interlayer coupling [17–19,21,22]. Inevitably, the interlayer interactions provide a new degree of freedom in band engineering and pave the way to create a new library of 3D structures for tunable optoelectronic properties with designed composite layers. However, accessing the optoelectronic properties of such heterostructures is challenging due to limited to micron scale lateral size or few layer thick samples obtained for the standard fabrication processes, such as mechanical exfoliation and chemical vapor deposition. Another possible method to fabricate larger heterostructures from 2D materials is by liquid phase exfoliation [19,23–25]. In this technique, a variety of layered compounds, including graphene and TMDs, can be efficiently dispersed in common solvents and deposited as individual flakes, or even as thin films. By mixing dispersions of different layered materials in specific ratios one can also form specific composites [18,26] , which can in turn be spray coated to form thick, robust films [18]. These robust thick films can exhibit novel opto-

electronic properties that can be engineered based on their 2D composition. Combined with their ease of production and scalability, they can be potentially useful for future opto-electronic devices. From that perspective, developing a deeper understanding of the photoconductive and opto-electornic response of such heterostructure films is an important avenue of study.

Previously, time resolved optical pump terahertz probe (OPTP) techniques have been shown to be powerful tools to access the dynamics of photocarriers, such as the time-resolved complex conductivity on photoexcitation, the lifetime of free carriers and the formation of bound states like excitons. [27,28]. In these techniques, typically a visible or near infrared probe pulse photoexcite the sample, which is then probed by a time-delayed, broadband THz pulse. By measuring the change in amplitude and phase of the transmitted (or reflected) THz pulse due to photoexcitation, one can access the time-resolved complex photoconducitivty of the sample. Recently, these techniques were used to study the change in performance of semiconductor opto-electronic devices due to laser ablation [29], as well as to understand the fundamental opto-electronic response of hBN/Graphene heterostructure laminates [18]. Using this technique to further study the complex photoconductive response of other vdW heterostructure laminates, particularly ones containing the optically active semiconducting TMDs, would provide an important contribution in understanding their utility in future optoelectronic devices.

In this work, we have fabricated WS_2 laminates, as well as heterostructure laminates formed from WS_2 and hexagonal boron nitride (hBN) (from here onwards termed as hBN/WS_2), and compared their photocarrier dynamics and frequency-resolved THz photoconductivity. We show that, despite the disordered nature of the stacking and orientations, novel macroscopic optoelectronic phenomena emerge from the microscopic interaction of the preserved 2D constituents, i.e. interfacial dipoles formation at the insulator-semiconductor interfaces in the hBN/WS_2 laminates. A combination of transmission electron microscopy (TEM) and photoluminescence (PL) measurements reveal that the laminates preserve the few layer optical response of the WS_2 and hBN/WS_2 samples. We compare the carrier recombination dynamics between WS_2 and hBN/WS_2 using optical pump-terahertz probe (OPTP). Whereas WS_2 shows a monotonic decay composed

of a slow and fast component, in the hBN/WS_2, an initial fast decay is followed by a 3.5 ps rise dominating the response. We attribute this effect to the decay of free carriers (drop in transmission) combined with an opposite sign contribution (increased transmission) originating from interfacial dipoles decay. In addition, we show that while the WS_2 complex photoconductivity can be well reproduced by a Drude-Smith response, the hBN/WS_2 response follows a Drude-Lorentz model including a dipole term.

Results and discussions

Artificial laminates of WS_2 and hBN/WS_2 are fabricated similarly to our previous work [18]. WS_2 and hBN few layer flakes are independently exfoliated in dimethylformamide via ultrasonic cleavage of high-purity powdered bulk crystals from Sigma-Aldrich. The resulting solution of exfoliated flakes is centrifuged at 10000 rpm to get a stable dispersion. These WS_2 and hBN dispersions are filtered and re-dispersed separately in tetrahydrofuran (THF) and then mixed together in 1:1 volume ratios. The hybrid flakes in the solution undergo van der Waals interactions that lead to the formation of hBN/WS_2 hybrid flakes. We spray coat these hybrid flakes onto a quartz substrate and allow for the solvent (THF) to evaporate. The procedure is repeated to form hybrid films of a few micrometer thicknesses with the specified composition on 1 square cm quartz.

TEM and Photoluminescence studies:

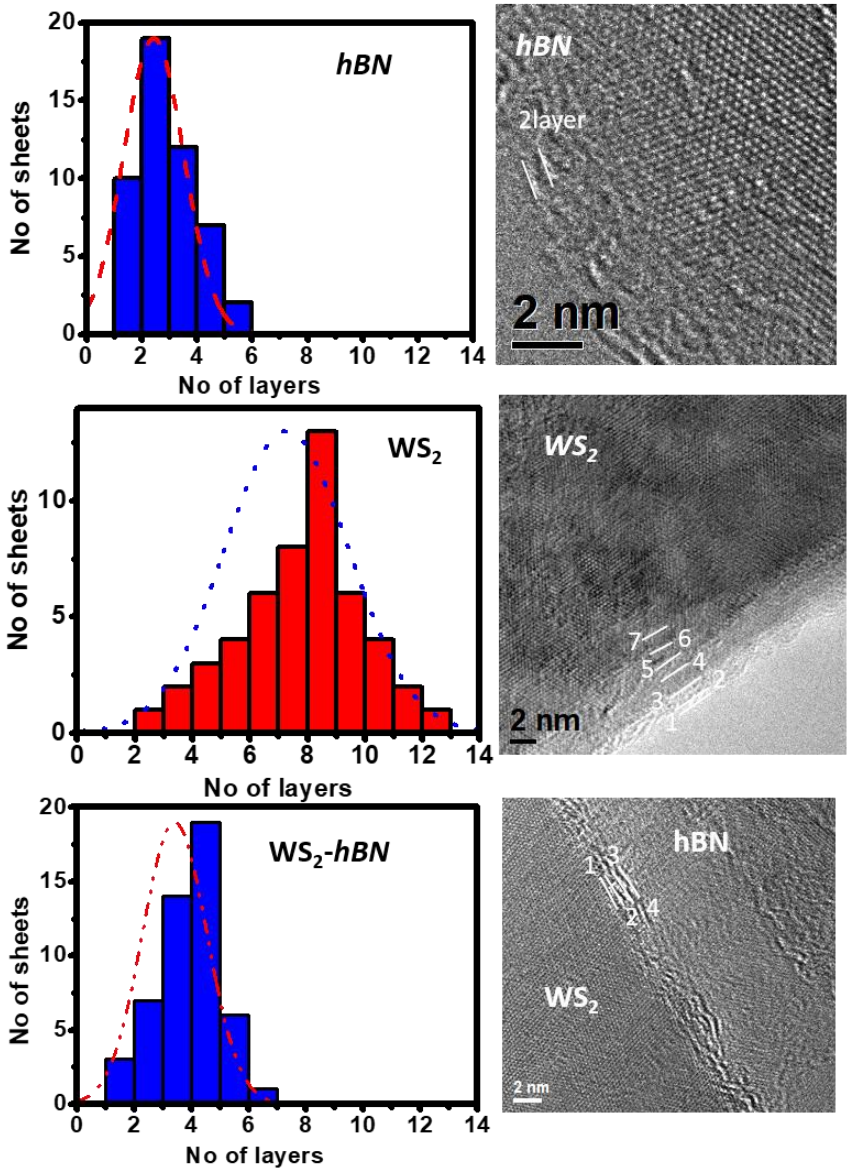

Figure 1. Left panels depict the average layer distribution of the flakes in hBN, WS_2, and hBN/WS_2. Right panels show TEM images of typical flake size obtained in the laminates.

The distribution of layers (average over multiple measurements) was determined by TEM studies of WS_2 and hBN/WS_2 flakes deposited on the carbon grid from the colloidal suspensions before they were used to make the thick laminates by spray coating. The left panels in Figure 1 show average distribution of layers in hBN, WS_2 and hBN/WS_2 samples. Spray-coating process formed 6-9 layers distribution in WS_2 by aggregation whereas hBN barrier layers minimize the layer distribution to 2-4 layers along with presence

of few monolayers in hBN/WS_2. The formation and configuration of layers in the laminates are shown in TEM images of Figure 1.

The room temperature photoluminescence spectrum excited with 532 nm CW laser for WS_2 and hBN/WS_2 laminates are illustrated in Figure 2. It has been shown that in WS_2, the PL spectra exhibits remarkable dependence on the number of layers such as blue shifting in an indirect gap peak emission and emission intensity enhancement when the thickness of the flakes is reduced [30,31]. Excitonic emission peaks A and B arise from direct bandgap transitions in WS_2 at the K points around 2 eV and 2.3 eV independent of the thickness and is in good agreement with previous studies [30–32]. The relative peak energy difference between indirect gap and the A-exciton in the bulk is ΔE_{bulk}~500 meV and decreases as the thickness of the flake is reduced [30,32]. In Figure 2, the laminates show strong and broad emission for indirect bandgap transition compared to the bulk [31,32], which indicates simultaneous emission from a distribution of few layers. In addition, the relative peak energies between the indirect and A-exciton are ΔE_{WS2} ~ 400 meV and $\Delta E_{hBN/WS2}$ ~300 meV and are in agreement with the distributions measured by TEM (hBN/WS_2 is composed of thinner layers). The enhanced emission in hBN/WS_2 (see inset of Figure 2) can be explained by a better quantum yield owing to the hBN intercalation and fewer layers.

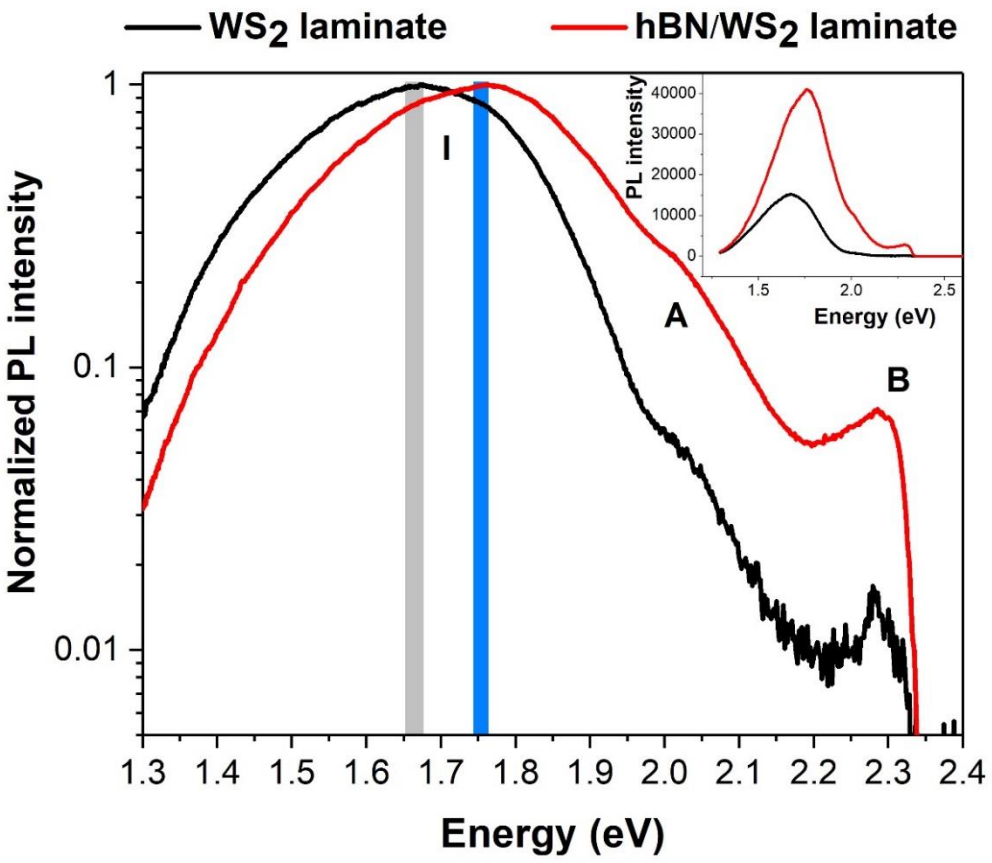

Figure 2. Normalized PL spectra of WS_2 and hBN/WS_2 laminates. Peak I-indirect gap emission and A & B are exciton peaks due to direct gap transition at the K-point. Inset shows the increase of PL intensity in hBN/WS_2 due to hBN intercalation

Photocarrier dynamics in the laminates:

To measure the photocarrier dynamics and terahertz photoconductivity in WS_2 and hBN/WS_2 laminates, we performed optical pump-terahertz probe measurements [27]. The pump is delivered by a 1 kHz Ti:Sapphire amplifier, frequency-doubled to 400 nm (3.1 eV) and attenuated to a fluence of 220 μJ/cm^2 (≈$10^{17}cm^{-3}$ photocarriers in the sample). The THz probe is generated via optical rectification in a ZnTe crystal and detected by electro-optic sampling provides a 0.5-2 THz bandwidth. The differential terahertz transmission (ΔT/T) is measured by parking the THz sampling delay line at the peak of THz field and scanned the pump delay line. Details of the technique used are described in [18]. This spectroscopy

technique allows not only access to the change in the transmitted probe amplitude but also to phase shifts as the THz pulse propagates through a medium. From that, one can extract the complex photoconductivity which gives the possibility to distinguish between the free charge carriers' and bound charges' (neutral) contributions [18,28,33,34]. The measured transient photo-induced terahertz transmission for WS_2 and hBN/WS_2 is depicted in Figure 3. In WS_2 laminate, the negative differential THz transmission signal decays on a fast time scale of few ps followed by a slow decay. The hBN/WS_2 shows an unusual response composed of an initial fast decay immediately followed by a fast rise.

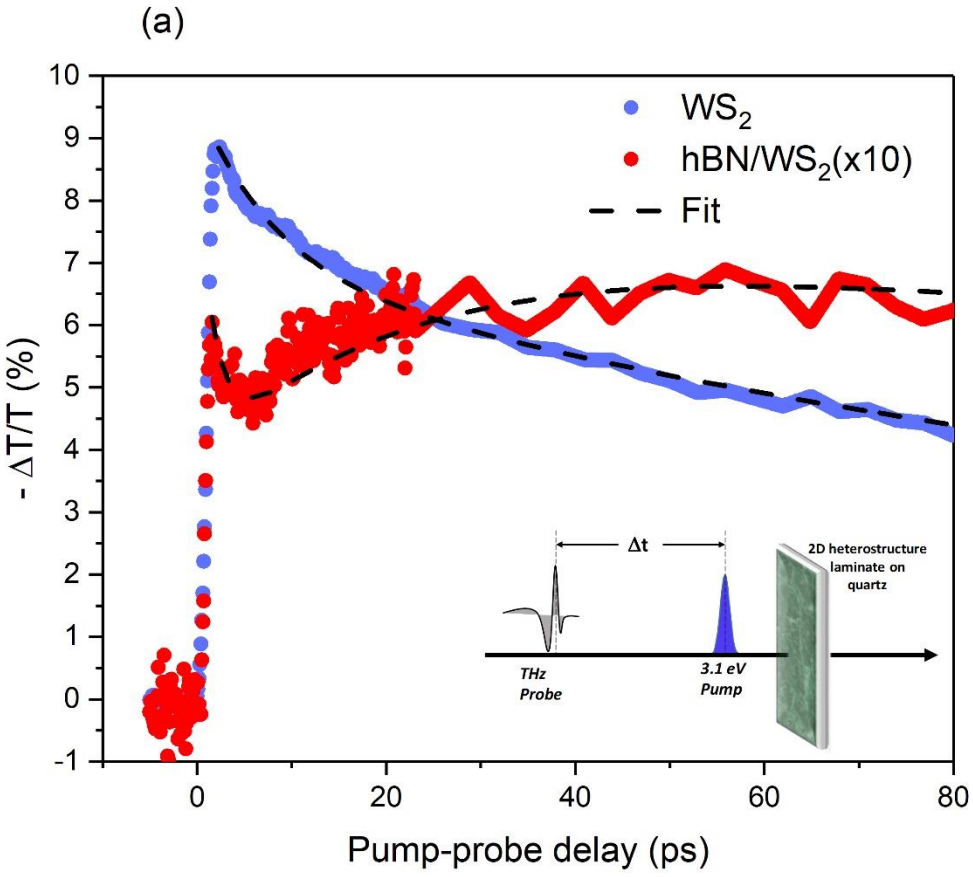

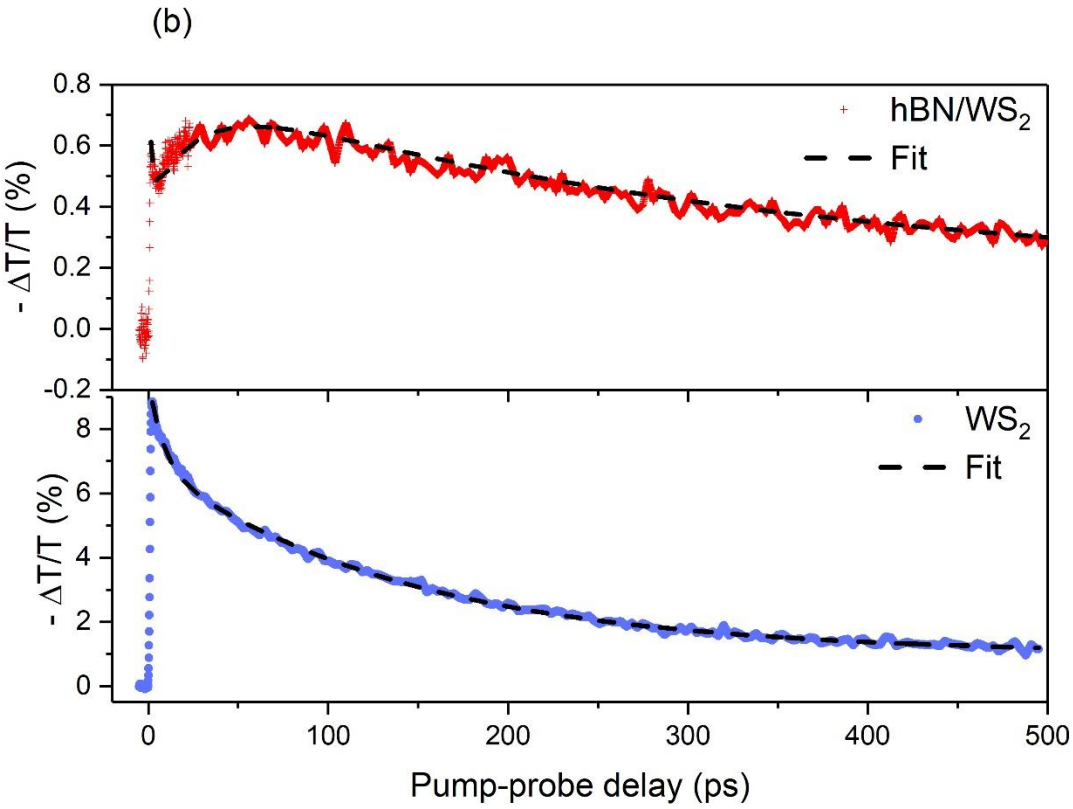

Figure 3. a) Negative differential terahertz transmission versus probe delay with respect to pump pulse for pure WS_2 and WS_2/hBN laminates. The pump fluence is 220 μJ/cm^2. b) Transient response over a 500 ps time window. Note: Step size was continuously increased from 100fs to 10 ps to optimize the acquisition time.

In Figure 3(a) and 3(b), the dashed lines correspond to fitting functions using exponential decays. The WS_2 transient response was fitted using a function of the form $Ae^{-t/T1} + Be^{-t/T2}$ from which we extract a short lifetime (8 ps) and longer lifetime (143 ps). The mechanisms dominating the charge dynamics in transition metal dichalcogenide laminates is known to be non-radiative like defect-assisted Auger recombination [35,36]. The hBN/WS_2 can only be fitted by a function of the form $Ae^{-t/T1} + Be^{-t/T2} - Ce^{-t/T3}$. The last term is a decay with negative amplitude. This component contributes as an increased THz transmission

after photoexcitation. From the fitting parameters, we extract values of 1.7 ps and 334 ps for T1 and T2, as well as T3 of 25 ps corresponding to the rise time.

Frequency-dependent terahertz conductivity of the laminates:

The frequency-resolved terahertz complex photoconductivity response is measured in the range from 0.5 THz - 2 THz. We acquire THz spectra at different pump–probe delays of Δt = 0, 8, 20 and 100 ps, corresponding to the instant of photoexcitation, the dip and the rise in the hBN/WS_2 and at later time delay, respectively. These time domain THz spectra were then Fourier transformed to frequency domain. From the information on the amplitude and phase of the Fourier transformed THz spectra, we can extract the pump-induced change of the complex photoconductivity, $\Delta\sigma$, at different time delays (see Fig. 4(a) and (b)). Details can be found in [18]. We estimate a penetration depth of around ~100 nm and is just a scaling factor for the photoconductivity. In reality most of the dynamics takes place within this length, however our calculated photoconductivities can be understood as effective conductivity of the few micron films. For the WS_2, we fit our data by using a Drude-Smith response [37]

$$\Delta\sigma_{WS2} = \alpha_{WS2} e^{-\Delta t/T_{WS2}} \frac{1}{1-i\omega\tau}\left(1+\frac{C_{WS2}}{1-i\omega\tau}\right) \qquad (1)$$

where α_{WS2} = 15 S cm^{-1}, Δt is the time delay, T_{WS2} = 140 ps is an average free carrier lifetime, τ=0.4 ps is the scattering time and C_{WS2}=-0.85 is the back-scattering parameter constant.

In the case of the hBN/WS_2, the previous model does not reproduce the experimental data. Instead, we use a Drude-Lorentz model that includes a dipole term. The temporal change of the complex photoconductivity can be expressed as:

$$\Delta\sigma_{hBN/WS2} = \alpha_{hBN/WS2} e^{-\Delta t/T_{WS2}} \frac{1}{1-i\omega\tau}\left(1+\frac{C_{hBN/WS2}}{1-i\omega\tau}\right) + L e^{-\Delta t/T_{Dipoles}}\left(\frac{1}{1-i\tau(\omega-\frac{\omega_0^2}{\omega})}\right) \qquad (2)$$

where $\alpha_{hBN/WS2}$=4 S cm^{-1}, L=0.9 S cm^{-1}, $T_{Dipoles}$=25 ps (as extracted from the transient data) and ω_0=12.5 THz is the resonant dipole frequency.

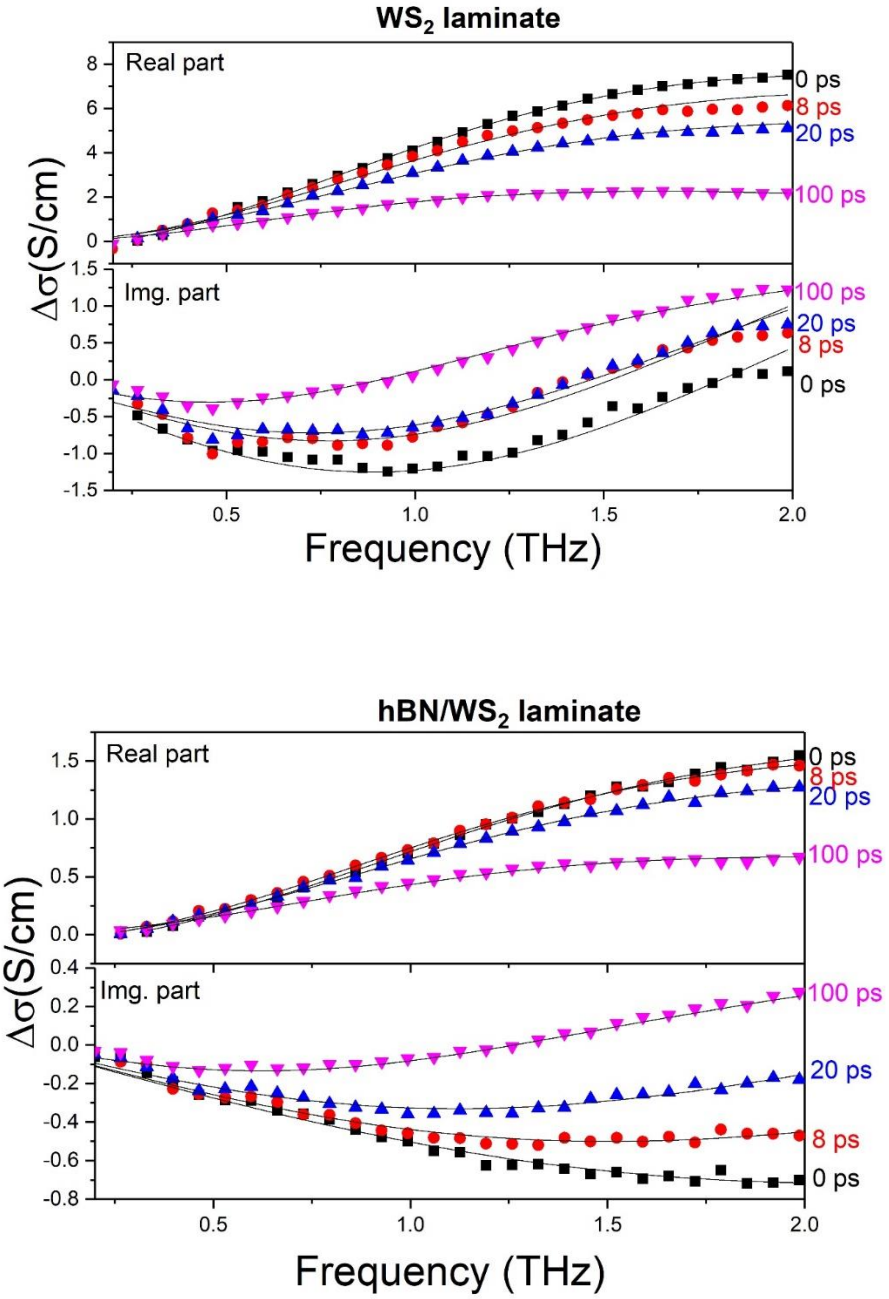

Figure 4. Terahertz complex photoconductivity spectra at 0, 8, 20 and 100 ps of (a) the WS_2 laminate and (b) the hBN/WS_2 structure. The solid lines correspond to fits obtained from equation (1) and (2).

The necessity of adding a dipole term to model the photo-response of the hBN/WS_2 heterostructure confirms the coexistence of two populations, free carriers and neutral dipoles. After photoexcitation, free carriers and dipoles decay at different rates and with opposite signs in the temporal response. As seen in Figure 4, the real part of the photoconductivity for the two compounds shows a similar trend. For the imaginary part, the two compounds have a different response from 0 to 20 ps and then become similar again at 100 ps. It shows that the dipole population mainly affects the imaginary part of the photoconductivity and can be understood as a transient change of refractive index, which results in an induced transmission component in the negative differential signal.

Conclusion:

We have fabricated large van der Waals heterostructures from 2D layers of WS_2 and hBN. These laminates preserve the few layer optical response. Moreover, the intercalation with hBN allows an average distribution of 2-4 layers. The hBN/WS_2 heterostructure also exhibit additional 2D properties like interface dipoles sensitive to photoexcitation even at a large 3D scale. The decay of those dipoles along with free carriers provides an additional way of altering and controlling the ultrafast response of a material. This feature, combined with the possibility of designing a large variety of heterostructures with various optoelectronic responses, is of importance to developing new devices such as THz phase shifters or modulators.

References:

[1] Geim A K and Grigorieva I V. 2013 Van der Waals heterostructures *Nature* **499** 419–25

[2] Hong X, Kim J, Shi S F, Zhang Y, Jin C, Sun Y, Tongay S, Wu J, Zhang Y and Wang F 2014 Ultrafast charge transfer in atomically thin MoS_2/WS_2 heterostructures *Nat. Nanotechnol.* **9** 682–6

[3] Yu Y, Hu S, Su L, Huang L, Liu Y, Jin Z, Purezky A A, Geohegan D B, Kim K W, Zhang Y and

Cao L 2015 Equally Efficient Interlayer Exciton Relaxation and Improved Absorption in Epitaxial and Nonepitaxial MoS_2 /WS_2 Heterostructures *Nano Lett.* **15** 486–91

[4] Rivera P, Schaibley J R, Jones A M, Ross J S, Wu S, Aivazian G, Klement P, Seyler K, Clark G, Ghimire N J, Yan J, Mandrus D G, Yao W and Xu X 2015 Observation of long-lived interlayer excitons in monolayer $MoSe_2$-WSe_2 heterostructures *Nat. Commun.* **6** 4–9

[5] Rigosi A F, Hill H M, Li Y, Chernikov A and Heinz T F 2015 Probing Interlayer Interactions in Transition Metal Dichalcogenide Heterostructures by Optical Spectroscopy: MoS_2/WS_2 and $MoSe_2$/WSe_2 *Nano Lett.* **15** 5033–8

[6] Ceballos F, Bellus M Z, Chiu H-Y and Zhao H 2015 Probing charge transfer excitons in a $MoSe_2$ –WS_2 van der Waals heterostructure *Nanoscale* **7** 17523–8

[7] Heo H, Sung J H, Cha S, Jang B G, Kim J Y, Jin G, Lee D, Ahn J H, Lee M J, Shim J H, Choi H and Jo M H 2015 Interlayer orientation-dependent light absorption and emission in monolayer semiconductor stacks *Nat. Commun.* **6** 1–7

[8] Rivera P, Seyler K L, Yu H, Schaibley J R J R, Yan J, Mandrus D G D G, Yao W and Xu X 2016 Valley-Polarized Exciton Dynamics in a 2D Semicondcutor Heterostructure *Science (80-.).* **351** 688

[9] Chen H, Wen X, Zhang J, Wu T, Gong Y, Zhang X, Yuan J, Yi C, Lou J, Ajayan P M, Zhuang W, Zhang G and Zheng J 2016 Ultrafast formation of interlayer hot excitons in atomically thin MoS_2/WS_2 heterostructures *Nat. Commun.* **7** 1–8

[10] Schaibley J R, Rivera P, Yu H, Seyler K L, Yan J, Mandrus D G, Taniguchi T, Watanabe K, Yao W and Xu X 2016 Directional interlayer spin-valley transfer in two-dimensional heterostructures *Nat. Commun.* **7** 1–6

[11] Ross J S, Rivera P, Schaibley J, Lee-Wong E, Yu H, Taniguchi T, Watanabe K, Yan J, Mandrus

D, Cobden D, Yao W and Xu X 2017 Interlayer Exciton Optoelectronics in a 2D Heterostructure p-n Junction *Nano Lett.* **17** 638–43

[12] Hunt B, Taniguchi T, Moon P, Koshino M and Ashoori R C 2013 Massive Dirac Fermions and *Science (80-.).* **340** 1427–31

[13] Ponomarenko L A, Gorbachev R V., Yu G L, Elias D C, Jalil R, Patel A A, Mishchenko A, Mayorov A S, Woods C R, Wallbank J R, Mucha-Kruczynski M, Piot B A, Potemski M, Grigorieva I V., Novoselov K S, Guinea F, Fal'Ko V I and Geim A K 2013 Cloning of Dirac fermions in graphene superlattices *Nature* **497** 594–7

[14] Dean C R, Wang L, Maher P, Forsythe C, Ghahari F, Gao Y, Katoch J, Ishigami M, Moon P, Koshino M, Taniguchi T, Watanabe K, Shepard K L, Hone J and Kim P 2013 Hofstadter's butterfly and the fractal quantum Hall effect in moiré superlattices *Nature* **497** 598–602

[15] Lee C H, Lee G H, Van Der Zande A M, Chen W, Li Y, Han M, Cui X, Arefe G, Nuckolls C, Heinz T F, Guo J, Hone J and Kim P 2014 Atomically thin p-n junctions with van der Waals heterointerfaces *Nat. Nanotechnol.* **9** 676–81

[16] Withers F, Del Pozo-Zamudio O, Mishchenko A, Rooney A P, Gholinia A, Watanabe K, Taniguchi T, Haigh S J, Geim A K, Tartakovskii A I and Novoselov K S 2015 Light-emitting diodes by band-structure engineering in van der Waals heterostructures *Nat. Mater.* **14** 301–6

[17] Fang H, Battaglia C, Carraro C, Nemsak S, Ozdol B, Kang J S, Bechtel H A, Desai S B, Kronast F, Unal A A, Conti G, Conlon C, Palsson G K, Martin M C, Minor A M, Fadley C S, Yablonovitch E, Maboudian R and Javey A 2014 Strong interlayer coupling in van der Waals heterostructures built from single-layer chalcogenides *Proc. Natl. Acad. Sci.* **111** 6198–202

[18] Krishna M B M, Man M K L, Vinod S, Chin C, Harada T, Taha-Tijerina J, Tiwary C S, Nguyen P, Chang P, Narayanan T N, Rubio A, Ajayan P M, Talapatra S and Dani K M 2015 Engineering

Photophenomena in Large, 3D Structures Composed of Self-Assembled van der Waals Heterostructure Flakes *Adv. Opt. Mater.* **3** 1551–6

[19] Gao G, Gao W, Cannuccia E, Taha-tijerina J, Balicas L, Mathkar A, Narayanan T N, Liu Z, Gupta B K, Peng J, Yin Y, Rubio A and Ajayan P M 2012 Arti fi cially Stacked Atomic Layers : Toward New van der Waals Solids *Nano Lett.* **12** 3518–25

[20] He G, Nathawat J, Kwan C P, Ramamoorthy H, Somphonsane R, Zhao M, Ghosh K, Singisetti U, Perea-López N, Zhou C, Elías A L, Terrones M, Gong Y, Zhang X, Vajtai R, Ajayan P M, Ferry D K and Bird J P 2017 Negative differential conductance & hot-carrier avalanching in monolayer WS_2 FETs *Sci. Rep.* **7** 1–9

[21] Perali A, Neilson D and Hamilton A R 2013 High-temperature superfluidity in double-bilayer graphene *Phys. Rev. Lett.* **110** 1–5

[22] Bokdam M, Khomyakov P A, Brocks G, Zhong Z and Kelly P J 2011 Electrostatic doping of graphene through ultrathin hexagonal boron nitride films *Nano Lett.* **11** 4631–5

[23] Coleman J N, Lotya M, O'Neill A, Bergin S D, King P J, Khan U, Young K, Gaucher A, De S, Smith R J, Shvets I V., Arora S K, Stanton G, Kim H Y, Lee K, Kim G T, Duesberg G S, Hallam T, Boland J J, Wang J J, Donegan J F, Grunlan J C, Moriarty G, Shmeliov A, Nicholls R J, Perkins J M, Grieveson E M, Theuwissen K, McComb D W, Nellist P D and Nicolosi V 2011 Two-dimensional nanosheets produced by liquid exfoliation of layered materials *Science (80-.).* **331** 568–71

[24] Nicolosi V, Chhowalla M, Kanatzidis M G, Strano M S and Coleman J N 2013 Liquid exfoliation of layered materials *Science (80-.).* **340**

[25] Huo C, Yan Z, Song X and Zeng H 2015 2D materials via liquid exfoliation: a review on fabrication and applications *Sci. Bull.* **60** 1994–2008

[26] Vinod S, Tiwary C S, Da Silva Autreto P A, Taha-Tijerina J, Ozden S, Chipara A C, Vajtai R, Galvao D S, Narayanan T N and Ajayan P M 2014 Low-density three-dimensional foam using self-reinforced hybrid two-dimensional atomic layers *Nat. Commun.* **5** 1–9

[27] Beard M C, Turner G M and Schmuttenmaer C A 2002 Terahertz spectroscopy *J. Phys. Chem. B* **106** 7146–59

[28] Richter C and Schmuttenmaer C A 2010 Exciton-like trap states limit electron mobility in TiO2nanotubes *Nat. Nanotechnol.* **5** 769–72

[29] Madéo J, Margiolakis A, Zhao Z-Y, Hale P J, Man M K L, Zhao Q-Z, Peng W, Shi W-Z and Dani K M 2015 Ultrafast properties of femtosecond-laser-ablated GaAs and its application to terahertz optoelectronics *Opt. Lett.* **40** 3388

[30] Zhao W, Ghorannevis Z, Chu L, Toh M, Kloc C, Tan P-H and Eda G 2013 Evolution of Electronic Structure in Atomically Thin Sheets of WS_2 and WSe_2 *ACS Nano* **7** 791–7

[31] Kim H-C, Kim H, Lee J-U, Lee H-B, Choi D-H, Lee J-H, Lee W H, Jhang S H, Park B H, Cheong H, Lee S-W and Chung H-J 2015 Engineering Optical and Electronic Properties of WS_2 by Varying the Number of Layers *ACS Nano* **9** 6854–60

[32] Zeng H, Liu G Bin, Dai J, Yan Y, Zhu B, He R, Xie L, Xu S, Chen X, Yao W and Cui X 2013 Optical signature of symmetry variations and spin-valley coupling in atomically thin tungsten dichalcogenides *Sci. Rep.* **3** 2–6

[33] Wang F, Shan J, Islam M A, Herman I P, Bonn M and Heinz T F 2006 Exciton polarizability in semiconductor nanocrystals *Nat. Mater.* **5** 861–4

[34] Kaindl R A, Hägele D, Carnahan M A and Chemla D S 2009 Transient terahertz spectroscopy of excitons and unbound carriers in quasi-two-dimensional electron-hole gases *Phys. Rev. B - Condens. Matter Mater. Phys.* **79** 1–13

[35] Kar S, Su Y, Nair R R and Sood A K 2015 Probing Photo-Excited Carriers in a Few Layer MoS Laminate by Time Resolved Optical Pump-Terahertz Probe Spectroscopy Probing Photo-Excited Carriers in a Few Layer MoS 2 Laminate by Time Resolved Optical Pump-Terahertz Probe Spectroscopy *ACSNano* 12004–10

[36] Strait J H, Nene P and Rana F 2014 High intrinsic mobility and ultrafast carrier dynamics in multilayer metal-dichalcogenide MoS2 *Phys. Rev. B - Condens. Matter Mater. Phys.* **90** 1–9

[37] Smith N V 2001 Classical generalization of the Drude formula for the optical conductivity *Phys. Rev. B* **64** 155106 1–6